Spectrogonio radiometer for the study of the bidirectional reflectance and polarization functions of planetary surfaces. 1. Design and tests

Olivier Brissaud, Bernard Schmitt, Nicolas Bonnefoy, Sylvain Douté, Patrick Rabou, Will Grundy, and Michel Fily

We have developed a spectrogonio radiometer to measure in the laboratory (−35 °C to +30 °C) the bidirectional reflectance and polarization distribution functions of various types of planetary material from the UV to the near-IR (310–4800 nm). The major, to our knowledge, novel feature of this instrument is that it is capable of measuring dark to translucent materials with a high degree of radiometric accuracy under most viewing geometries. The sample surface is illuminated with a large monochromatic and polarized parallel beam (incidence: 0°–90°), and the total intensity and the two polarized components of the reflected light are measured (observation, 0°–80°; azimuth, 0°–180°). The scientific and technical constraints, the design, and the performances and limitations of the system are presented in this first paper.

OCIS codes: 120.4570, 120.5820, 290.5880, 300.6340, 300.6550.

1. Introduction

A. Scientific Problematics and Objectives

With current and future space missions, imaging spectrometers provide hyperspectral images of planetary surfaces under variable illumination and observation geometries. These remote-sensing data require laboratory data of spectral bidirectional reflectance and radiative transfer models describing the different observational conditions to accurately retrieve the surface composition, texture, roughness, etc. However, there are currently no accurate enough measurements of the spectral bidirectional reflectance distribution function (spectral BRDF) on sufficiently well-characterized granular and compact surfaces to validate these models. Moreover, these models often include ill-known parameters such as the single-scattering albedo and phase function, as well as the opposition parameters.[1–3] For materials such as ices and minerals, most of these parameters are completely unknown or determined semiempirically. The parameters of the scattering phase function are frequently set to a constant, independent of the wavelength and the optical constants of the grain surface material. Our recent Monte Carlo simulations for irregular grains show that this function strongly depends on the real and imaginary indices as well as on the size, shape, and surface roughness of the grains.[4]

In addition, the polarization of the light reflected by a granular surface is currently almost unexploited because it is still poorly experimentally studied and theoretically not well understood. For a few materials there are some empirical relations between characteristic features of the polarization curve and surface properties (albedo, compactness, etc.), but they do not yet have satisfactory theoretical explanations.[1]

Consequently, we have designed a specific instrument (called a spectrogonio radiometer) to study in the laboratory the light-scattering properties of plan-

O. Brissaud (olivier.brissaud@obs.ujf-grenoble.fr), B. Schmitt, N. Bonnefoy, and S. Douté are with the Laboratoire de Planétologie de Grenoble, Centre National de la Recherche Scientifique—Université Joseph Fourier, Bâtiment D de Physique, B.P. 53, 38041 Grenoble Cedex 9, France. P. Rabou is with the Laboratoire d'Astrophysique, Centre National de la Recherche Scientifique—Universite Joseph Fourier, 414 rue de la Piscine, BP 53, 38041 Grenoble Cedex 9, France. W. Grundy is with Lowell Observatory, 1400 West Mars Hill Road, Flagstaff, Arizona 86001. M. Fily is with the Laboratoire de Glaciologie et Géophysique de l'Environnement, Centre National de la Recherche Scientifique, 54 rue Molière, B.P. 96, 38402 Saint Martin d'Hères Cedex, France.

Received 21 February 2003; revised manuscript received 17 November 2003; accepted 10 December 2003.

0003-6935/04/091926-12$15.00/0

etary surfaces. The main objectives are to understand the spectral reflectance behavior and the polarization effect of granular and compact surfaces in the visible and near IR under any viewing geometry (angles of illumination, reflection, and azimuth) in order to test, improve, and validate the existing numerical models. In particular, we intend to measure the spectral bidirectional reflectance and polarization functions of snows with different physical parameters such as grain size and shape, compactness, surface roughness, and stage of metamorphism. Moreover, polarized reflectance measurements of several types of material (rocks, minerals, ices, organics, etc.) will supply a BRDF database that should provide useful information for the data interpretation of the current and future space missions (Galileo, Cassini, Mars missions, Rosetta, etc.) and Earth observer satellites (Systeme Pour l'Observation de la Terre, Landsat, Advanced Earth Observing Satellite, Terra, etc.).

B. Existing Instruments

Various goniometers have been already designed for specific applications. They can be split into two groups of instruments: (1) devices designed to measure samples at near-zero phase angles (angle between the detector optical axis, sample center, and illumination source) and (2) setups used to obtain information over a large spectral range with various angles of incidence and reflection. In the following, we briefly review the major existing instruments.

1. Instruments to Study the Opposition Effect

An original device is the long-arm goniometer of the Jet Propulsion Laboratory (USA). The angles of incidence and emission can vary from 0° to 90°. It mainly consists of a He–Ne laser source modulated by a chopper and a p-i-n diode detector mounted at the end of a movable arm. A beam splitter is used to reach phase angles as small as 0°.[5] Recently the beam splitter was replaced by a mirror and quarter-wave plates, and linear polarizers were inserted into the incident and reflected light beams to study the changes in the circular polarization ratio with phase angle.[6,7] A similar system was designed at the University of Helsinki, Finland, to study the opposition effect.[8] A beam splitter is also used to reach zero phase angle. The light source is a He–Ne laser, but the detector is a CCD camera.

2. Polyvalent Spectrogoniometers

The Reflectance Experiment Laboratory (RELAB) goniometer (Brown University, USA)[9] was designed to study the light-scattering properties of granular surfaces. It allows measurement of the bidirectional reflectance of surfaces from 450 to 2600 nm under various illumination and observation angles (0°–60° for the incidence and emergence angles and 12°–120° for the phase angle range). The sample is illuminated by unpolarized monochromatic light, and the reflected light is measured by two detectors (visible: photomultiplier; IR: InSb).

Another device is the European Goniometric Facility[10,11] at the Joint Research Centre (Ispra, Italy). It is a large goniometer constructed to obtain bidirectional reflectance data on vegetation. The structure consists of two horizontal circular rails approximately 4 m in diameter on which two vertical arcs of 2 m in radius each can rotate. The first arc supports the light source, and the second arc holds the spectroradiometer (nominally 300 to 2500 nm but limited to 400–1000 nm in practice because of low signal-to-noise (S/N) ratio in the mid-IR region).[11] A similar system (Field Goniometer System[12]) with a lighter structure was designed at the University of Zurich, Switzerland. It is a transportable goniometer specially built for *in situ* target measurements under natural light conditions. Another transportable goniometer is the automated spectrogoniometer[13] designed to measure the spectral bidirectional factor of snow from 400 to 2500 nm. The automated spectrogoniometer has a two-link spherical robot coupled with a field spectroradiometer.

Another interesting goniometer designed to study natural surfaces such as sand or grass is the instrument of the Office National d'Etudes et de Recherches Aérospatiales (Toulouse, France).[14,15] The source is a quartz tungsten halogen lamp, and the reflected flux is collected by a fiber-optic bundle and sent in a spectrometer covering the 420–950-nm range. The main limitation is the angular domain (0°–60° for the source and sensor zenith angles).

A different device is the goniometer designed at the Deutsche Forschungsanstalt für Luft- und Raumfahrt (DLR) of Berlin, Germany, which was mainly planned for mineral sample measurements in support of space missions.[16] The system is built with two arms, allowing selection of the incident and the scattering directions. A spectroradiometer (250–2500 nm) directly mounted on the detection arm is used to measure the reflected light. It has similar angular limitations.

Although the design of our system was partly inspired by some of these goniometers, it was mainly conditioned by a number of specific scientific constraints. These constraints are essentially dependent on the application field (type of samples, angular and spectral ranges, etc.) and on the radiometric accuracy expected for the spectral and bidirectional reflectance measurements. Our main aim was to be able to measure dark to translucent materials with a high degree of radiometric accuracy over wide angular ranges. These considerations are presented in detail in Section 2. The design of the whole system that emerged from the technical analysis of these constraints is detailed in Section 3. Last, Section 4 describes the performance and limitations of the system. The calibration protocols of the reflectance measurements will be developed in a following paper referred to Part 2.[17]

2. Scientific Constraints

The main scientific constraints described in this section are connected to the spectral, geometric, and radiometric accuracies. Their analysis led us to define a set of ideal, nominal, and degraded values of the technical parameters to facilitate the choice of the compromises during the design of the system. At some point in this study, it appeared that the use of a monochromatic light source and broadband detectors instead of a broadband source and a spectrometer allowed us to overcome several problems encountered by previous systems. The main advantages are (1) a low input power on the sample (snow, etc.), (2) all mobile parts (monochromator, mirrors) on a fixed optical table, (3) a robust detection system (no polarization effects, no moving parts, transmission optics), and (4) a lighter goniometer.

A. Constraints of the Sample

The choice of the sample materials that will be studied is related to their planetary and terrestrial interest, to their radiometric properties, and to their availability and stability. The size of the sample must be large enough to simulate an infinite surface. Consequently, the radiometric errors induced by the limited size of the sample, compared with an infinitely large sample, must be negligible.

To estimate these errors, we developed an experiment and a numerical model to study the lateral scattering of light in granular samples (see Subsection 2.D). The results of this study showed that the sample should be 300 mm in diameter and 150 mm deep in the most unfavorable case (transparent material with millimeter-sized grains) to keep the radiometric error below 0.2% at all angular configurations. Another constraint that had to be taken into account during the system design is the low temperature (-35 °C) required by some samples (snow, ices, hydrates, etc.) to guarantee their radiometric stability over the duration of the measurements (typically, a few hours to a few days).

B. Spectral Constraints

Ideally, the spectral range of the instrument should cover the solar spectrum (150–5000 nm) reflected by planetary surfaces. A minimum range from 800 to 3000 nm is requisite as the main absorption bands of planetary surfaces appear in this spectral interval. Furthermore, spectral resolution and sampling should not undersample these bands. The ideal resolution for a sample would be less than one fifth of the FWHM of its narrower bands, i.e., 5–10 nm for H_2O ice and most minerals and 1 nm for most of the other planetary ices (e.g., molecular solids such as CO_2, CH_4, and SO_2). The wavelength precision and the monochromaticity of the light must be compatible with the resolution. The contribution of stray light at other wavelengths must be kept within the radiometric error requirement (see Subsection 2.F), in particular in spectral ranges in which strong absorption bands occur.

C. Angular Constraints

The illumination and observation angles of the goniometer should permit measurement at all geometric configurations of surface remote sensing. In other words, the illumination angle (θ_i) must vary from 0° to 90°, the observation angle (θ_r) must vary form 0° to +90°, and the azimuth angle (Φ) must vary from 0° to 180° (see Fig. 3). We would like to approach these theoretical limits, but, as we will see in Subsection 2.E, observations at high radiometric accuracy are extremely difficult above 80°. Some measurements at small phase angles ($g < 10°$) should also be possible to study the opposition effect. Finally, for accurate simulation of the bidirectional reflectance configuration, the divergence of the incident light beam and the field of view of the detector optics should be as small as possible. The angular resolution and sampling of the observation should be smaller than the width of the narrower reflectance feature (i.e., the specular peak, typically 5°–10° wide). Given the granular nature of the sample surfaces, absolute and relative angular accuracies better than 0.5° and 0.1°, respectively, are sufficient.

D. Constraints on the Illumination

The problem is similar to that of the size of the sample: The incident-beam diameter must be large enough to simulate an infinitely illuminated surface. To specify this constraint, we designed an experiment to measure the horizontal scattering distance of light within granular samples. This experiment used a He–Ne laser (light source) operating at 632 nm and a silicon photodiode (1 mm × 1 mm) to measure the light escaping from the surface in all directions as a function of the distance from the center of the laser spot (diameter: 2 mm). The measurements were made in a cold room at -15 °C with a sieved sample of artificial snow (grain size: 1–1.5 mm). This experiment was considered as the worst case (large grain sizes, low absorption coefficient) for lateral scattering. The data were fitted by an analytical function, extrapolated in the laser spot region (in which no measurement could be taken), taking into account the energy conservation (negligible absorption), and normalized to produce the point-spread scattering function of the sample material at 632 nm. A numerical model was then developed and used to convolve this function with various homogeneous incident beams (diameter D_i) and a set of observation diameters (D_o). In this way, the radiometric error relative to an infinitely large illumination was calculated for different beam sizes as a function of the observation angles (Fig. 1). These calculations were performed for nadir illumination, the most restricting configuration. A diameter of 200 mm was selected to keep the limited-illumination error for the worst snow sample below 0.2% for all θ_i and Φ and for $\theta_r < 75°$. Ideally, the illumination should be highly homogeneous within the beam and should be either unpolarized over the whole spectral range or fully polarized (extinction ratio $< 10^{-4}$) with the choice of

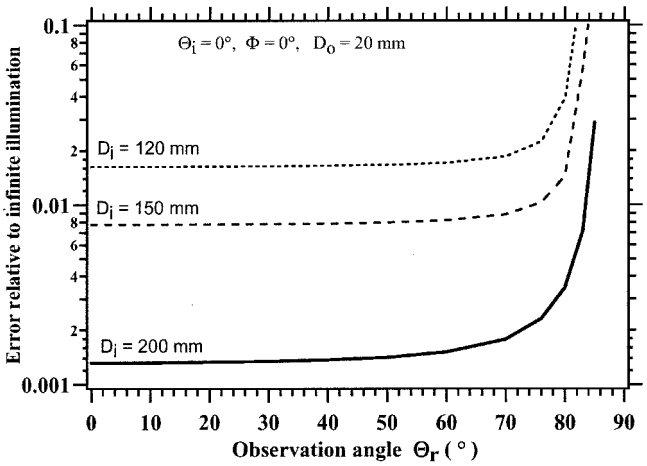

Fig. 1. Radiometric error relative to an infinitely large illumination beam for three illumination beam sizes D_i and for an observation footprint with diameter D_o = 20 mm, in the case of large-grained snow (1–1.5 mm) at 632 nm (worst-case study).

at least two perpendicular orientations of the polarization plane. Although we would prefer unpolarized illumination, as for the solar radiation (outside of the atmosphere), fully polarized configurations must at least be considered an option.

E. Constraints on the Observation

The observation diameter must be such that it does not introduce large radiometric errors at high observation angles (see Fig. 1) when the observation ellipse extends close to the border of the illumination beam ($D_o/\cos\,\theta_r \approx D_i$). At the same time, the observed sample area must be large enough to view a statistically sufficient number of surface grains. The best compromise was found to be 20 mm in diameter, allowing observations to as much as 80°–83° and sampling a few hundred 1-mm-sized grains at nadir. The nominal field of view selected (±2°) is a compromise between high angular resolution and S/N ratio, especially in the UV and IR ranges. Optional narrower fields of view should be available over restricted spectral ranges for high angular resolution studies (specular peak, etc.). An additional configuration allows measurement of the two polarized components of the reflected light under any viewing geometry. Ideally, the extinction ratio should be less than 10^{-3} from 300 to 5000 nm.

F. Radiometric Constraints

One of the main objectives of this new instrument is the measurement of the bidirectional reflectance of surfaces with a high degree of radiometric accuracy over large spectral and angular ranges and samples having optical properties varying from highly transparent to strongly absorbing. The limitation of the systematic errors due to the illumination and viewing geometries of the sample directly results from all the previous constraints. With the combined choice of sample size, illumination, and observation diameters, we succeeded in limiting the radiometric errors, relative to the ideal case of an infinitely large illumination beam, to less than 0.15% over most angular configurations in the worst-sample case (see Fig. 1). In a limited number of configurations (near-nadir illuminations), the upper limit for this error can reach 0.35% at θ_r = 80° and 1% at 83°. Numerical simulations showed that all these errors are strongly reduced as soon as the sample begins to absorb or for smaller grain sizes (less than a few hundred micrometers). However, we will see in Section 4 that the characteristics of the optical components and electronic devices making up the spectrogonio radiometer significantly increase the radiometric errors. It will then be necessary to develop specific calibration protocols to correct the main sources of errors. These procedures will be described in Part 2.[17]

3. Spectrogonio Radiometer Description

A. Technical Constraints

In addition to the scientific spectral, angular, and radiometric constraints, there are a number of technical constraints, either implied by the former or set by system-component availability, stability, and cost, that force the design of the whole system. The first major constraint is the availability of optical materials able to cover the whole spectral range from the UV to the mid-IR (<5000 nm) with a minimum of component changes during a scan in order to reduce complexity and sources of nonreproducibility. The second is the removal in the measured signal of the thermal IR radiated by the sample and the environment. The low temperature (−35 °C) needed for some samples and the impossibility, for radiometric reasons, of placing a window between the surface and the illumination and observation imply that at least the goniometer and the optical components fixed on its arms should operate at the cold chamber temperature. Finally, the stability of these samples also requires the use of low-illumination input power from the illumination.

To satisfy all these constraints, the system uses a modulated monochromatic light source (*illumination*) to illuminate the sample surface with two detectors (*observation*) to directly measure the reflected light (Figs. 2 and 3) at incident and scattering directions specified by the goniometer. The source components are placed on a fixed optical table in a temperature-controlled box and are flexibly connected with fiber optics to an illumination mirror on the goniometer. This design avoids the photometry and stability problems inherent in the rotation of the monochromator and to the collection of polarized reflected light by polarization-sensitive components (cf. RELAB[9] and DLR[16] goniometers). A *software* package controls the different motors and instruments and records the bidirectional spectra and several environmental parameters. A detailed description of these four parts is given below. The instrument's characteristics are summarized in Table 1.

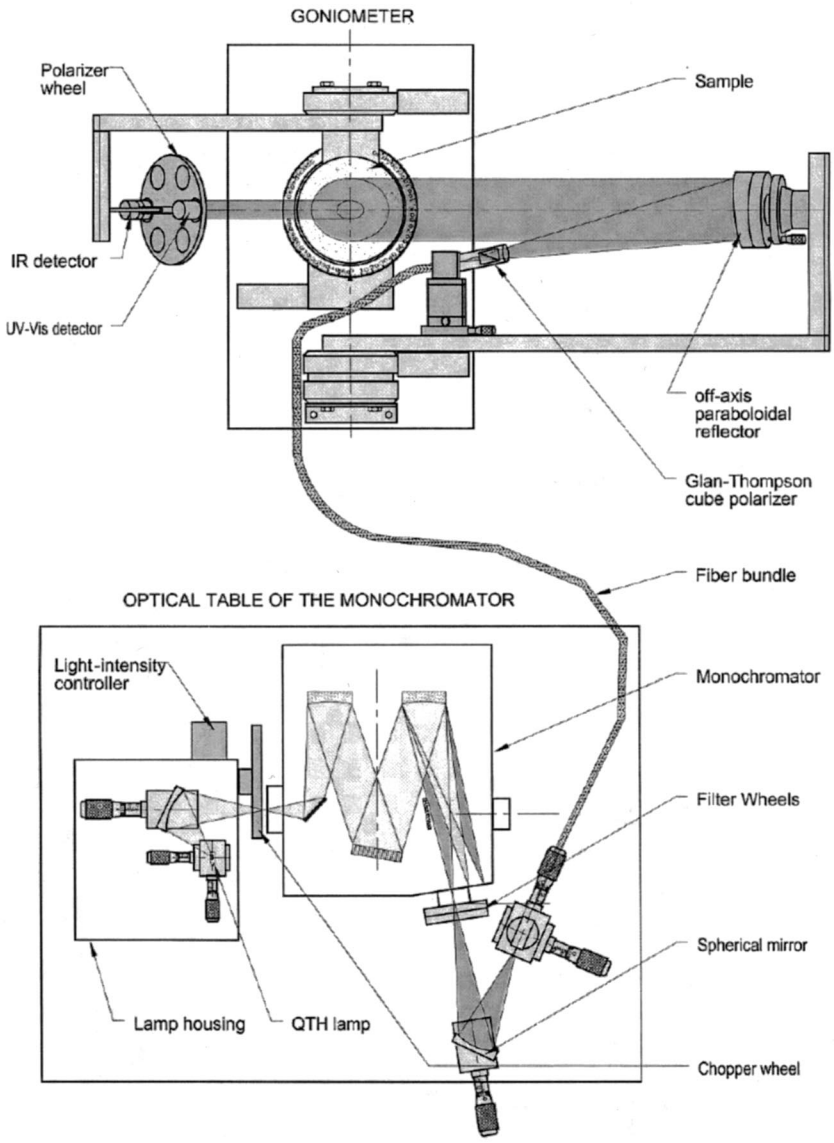

Fig. 2. Schematic drawing of the optical design of the spectrogonio radiometer. Vis, visible; QTH, quartz tungsten halogen.

B. Illumination

The light source illuminates the sample surface with a linearly polarized and parallel monochromatic beam. Light from a 250-W quartz tungsten halogen lamp, mounted in a lamp housing, is collected by a concave spherical mirror and focused onto a monochromator motorized input slit (variable width from 4 μm to 2 mm; height: 15 mm). The lamp housing includes a temperature-stabilized photodiode that constantly measures the light output of the lamp and adjusts the power-supply setting to compensate for any light-intensity variations. This system provides a highly stable long-term output (light variations $<$ 0.1% peak to peak over 24 h). A chopper wheel with an adjustable frequency is placed between the spherical mirror and the monochromator slit to modulate the light beam. This modulation allows the use of synchronous detection measurement to improve the detection limit of the detectors and to remove from the signal all light not originating from the source, especially the thermal IR emission from the sample and some optical parts. The monochromator (ORIEL MS257) has a $F/\#$ of 3.9. It incorporates a quadruple grating turret (1200, 600, 300, and 150 lines/mm) to cover the spectral range from 220 to 9000 nm and two filter wheels (after the exit motorized slit) with six long-pass filters to eliminate the higher orders. Two broad UV–visible bandpass filters have also been added to eliminate most of the stray light disturbing the low signal measurements below 450 nm. At the output of the monochromator, a concave spherical mirror collects the monochromatic flux and forms a 2X-reduced image of the exit slit on a fiber-optic bundle (Le Verre Fluoré). The 1.7-m-long bundle contains nine fluoride glass fibers with excellent transmittance from 300 to 4700 nm. The fibers are aligned at one end (input) to match the slit image and are arranged in a circle (diameter:

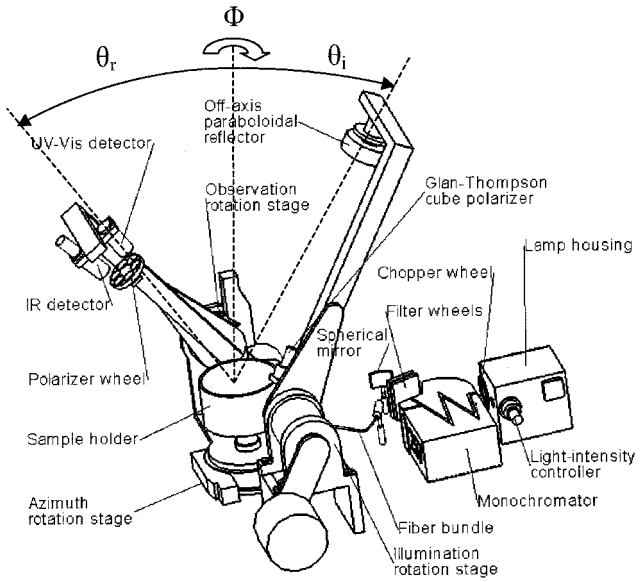

Fig. 3. Schematic three-dimensional view of the spectrogonio radiometer.

2.5 mm) at the other end (output). The fiber core diameter, 0.75 mm, determines the maximum output slit width (1.5 mm) and, accordingly, the largest spectral bandpass for each grating. The fiber bundle flexibly carries the light to the focal point of an off-axis paraboloidal reflector (diameter: 200 mm; f = 750 mm) placed on the illumination arm of the goniometer (see Subsection 3.D). This mirror illuminates the sample surface at a distance of 1000 mm with a large (200 mm in diameter) and highly parallel beam (divergence $< 0.1°$). A Glan–Thompson cube polarizer, fixed to a rotation stage, can be placed at the output of the fibers, and its polarization plane can be rotated between 0° and 90°.

This cube polarizer is made of $CaCO_3$ and has an extinction ratio of 10^{-5}. It has acceptance angles larger than the $\pm 7.5°$ required to fill the paraboloidal reflector. However, its spectral range is limited from 300 to approximately 3000 nm. An extension to as much as 5000 nm with a cube polarizer made from an IR birefringent crystal such as YVO_4 is envisaged. A large reference silicon photodiode (diameter: 28 mm) fixed to the illumination arm by a rotation stage can be positioned perpendicular to the center of the illumination beam to monitor its variations in the visible range averaged over an area similar to that of the observation spot at small-to-medium emergence angles (it contains the spot for $\theta_r \leq 36°$ and all Φ) (see Section 4). The addition of a second but much smaller reference detector for the IR range is planned.

C. Observation

The radiance of the sample is measured by two detectors: a silicon photodiode with a spectral response from 185 to 1200 nm and an InSb photovoltaic detector covering the spectral range from 800 to 5200 nm. The IR detector is cooled to 80 K by a Stirling microcooler (EG&G, RC3), and a cold diaphragm is used to restrict the field of view of the thermal background radiation to improve the S/N ratio. The modulated signals are amplified by current-to-voltage preamplifiers and measured by lock-in amplifiers (OPTILAS, SR 830). Each detector is fitted with a four-element achromatic condenser to collect the radiance of a small sample area within a narrow solid angle (see Subsection 2.E). Their measured spatial responses have cylindrical shapes 20 mm in diameter, and their angular responses have truncated cone shapes with FWHM of 4.1° and width at maximum of 2.9°. This solid angle ($\pm 2.05°$) defines the nominal instrument angular resolution. When necessary, one can achieve better angular resolutions by inserting a diaphragm (10 mm $\equiv$ 0.42°) in front of the detector optics, but this can be to the detriment of the S/N ratio. The two detector assemblies are fixed to the observation arm of the goniometer and are separated by 10° in the principal plane. Their distance to the sample is 700 mm. A polarizer wheel with four linear polarizers and two holes (unpolarized measurements) is placed in front of the detector optics. Three different dichroic polarizers are used to cover the range from the UV to the very near IR (extinction ratio $< 10^{-3}$), and grid polarizers are used to extend the range from the near to mid-IR. Two of these IR polarizers are mounted in series to improve the extinction ratio (1.3×10^{-3} at 1500 nm and 1.4×10^{-4} at 3000 nm). With this configuration, only one polarization component is measured over the whole spectral range, and the second component is deduced from the unpolarized measurements. It is also possible to directly measure both components, but over a reduced spectral range, by use of pairs of orthogonal polarizers.

D. Goniometer

The goniometer is designed and constructed from three rotation stages (Micro-contrôle) allowing rotation of the illumination arm from 0° to 90° incidence (θ_i) and of the observation arm from 0° to 90° for the zenithal angle (θ_r) and from 0° to 180° for the azimuth (Φ) (Fig. 3). All axes are driven by stepper motors with 0.001° increments. The position repeatability is 0.002°, and the rotation speed is $2° \ s^{-1}$. A counterweight is used for each arm to reduce the rotation torque. The structure and the different sample holders of the goniometer are anodized black to minimize the effects of stray light in the visible. The center of the sample surface is placed at the intersection point of the three rotation axes. A small motor is available under the sample holder to permit a slow continuous rotation of the sample (<10 rpm). This rotation may be used to increase the statistic of the particle geometries viewed by the detectors in the case of large particle sizes. The main geometric limitation of the system is the phase angle. Reflectance measurements are strongly perturbed at small phase angles because the shadow of the detectors in the illumination beam increases as the phase angle de-

Table 1. Instrument Characteristics

Characteristics	Quantities
Spectral characteristics	
Range unpolarized	310–4800 nm (measurable signal) 380–3900 nm (S/N > 100 in 1 s)
Polarized illumination	320–3000 nm
Polarized observation	320–4800 nm
Resolution	Minimum: <0.1 nm (but S/N limited) Maximum: 6 nm (<500 nm), 12 nm (<1000 nm), 24 nm (<2000 nm), 48 nm (>2000 nm)
Wavelength accuracy	0.2–0.6 nm (grating dependent)
Angular characteristics	
Incidence angle (θ_i)	0°–90° Resolution: 0.1° Maximum sampling: 0.1°
Emergence angle (θ_r)	0°–80° (to 83° for dark or fine-grained samples) Resolution: ±2° (may be reduced to <±0.5°, but S/N limited) Maximum sampling: 0.1°
Azimuth angle (Φ)	0°–180° Resolution: ±2° (may be reduced to <±0.5°, but S/N limited) Maximum sampling: 0.1°
Phase angle (g)	g_{min} to 165° g_{min} = 8° for bright or large-grained samples g_{min} = 4.5° for dark or fined-grained samples
Reproducibility	0.002°
Illumination characteristics	
Diameter (nadir)	200 mm
Parallelism	<0.1°
Homogeneity	±1% within 60-mm diameter ($\theta_r < 70°$) ±4% within 120-mm diameter ($\theta_r \leq 80°$)
Observation characteristics	
Detectors	Si (300–1200 nm) (room temperature) InSb (800–4800 nm) (cooled 80 K)
Diameter (nadir)	20 mm
Field of view	±2.05° (may be reduced to ≤±0.5°)
Radiometry	
Absolute accuracy	(see Part 2[17]) <1%, 400–1000 nm, % Spectralon (fully calibrated) <2%, 1000–2500 nm, % Spectralon (partly calibrated) <?%, 2500–4800 nm, % sulfur (under calibration)
Relative accuracy	<0.5% (400–2500 nm)
Polarimetry (optional)	
Illumination	Linear polarization: variable 0° to 90° Extinction ratio: 10^{-5}
Observation	S and P components Extinction ratio: $<10^{-3}$
Samples	
Type	Rocks, minerals, snow or ice, etc. (from bright to dark)
Texture	Compact or granular
Grain size	Micrometer to a few millimeters
Size	Maximum: 300-mm diameter, 250-mm deep (translucent and coarse grained) Maximum: 120-mm diameter, 2–10-mm deep (dark or fine-grained samples) Minimum: 25 mm × 120 mm ($\theta_r \leq 80°$, all Φ) Minimum: 25 mm × 45 mm ($\theta_r \leq 60°$, all Φ)
Temperature	Room temperature or heated Down to −35 °C (in cold room)

creases, up to the point at which it affects the radiance measured in the observation spot. This is particularly critical for coarse-grained transparent samples, such as snow in the visible, with a wide point-spread scattering function. In this case the minimum acceptable phase angle is 8° (see Part 2[17]). However, for much smaller grain sizes or at absorbing wavelengths, it will be possible to perform measurements down to 4.5° without significant radiometric error.

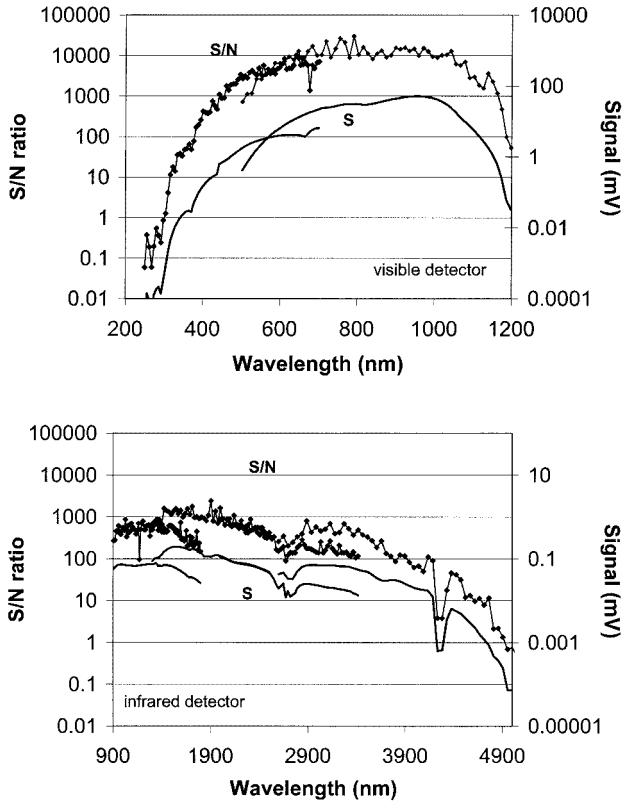

Fig. 4. Signal (S) and signal-to-noise (S/N) ratio (calculated from 25 individual measurements) for the visible and IR detectors (slit width = 1500 μm, time constant of the lock-in amplifier = 1 s, θ_i = 0°, θ_r = 15°). Spectralon and annealed sulfur panels,[18] with reflectance close to 1, are used to cover the 250–5000-nm range.[18] Overlapping curves correspond to different gratings. Absorptions around 2700 and 4250 nm are due to atmospheric H_2O and CO_2.

E. Software

Instrumentation software based on LabVIEW (National Instruments) with a general-purpose interface bus board is used to drive the spectrogonio radiometer, to define all the acquisition parameters, and to record and display the data through interactive front-panel user interfaces. The program drives the monochromator (gratings, slits, filter wheels), the Glan–Thompson cube polarizer (stepper motor), the reference detector, the polarizer wheel, the goniometer (three stepper motors), and the two lock-in amplifiers. The acquisition parameters (spectral range, resolution and sampling, angular range and sampling, polarizations, integration time, calibration steps, etc.) can be flexibly defined and optimized, allowing different types of experiment to be specified (single wavelength–full angular configurations, fixed geometry–full spectrum, spectra at fixed phase angle, etc.). The program defines the optimum sequential ordering of the geometrical configurations and records the detector signals as well as several environmental parameters (time, detector temperatures, sample temperature, lamp flux, etc.) for all spectral–angular configurations. Another software package written with the programming language IDL has been developed to reduce, calibrate, and display a set of spectral bidirectional reflectance measurements stored in four-dimensional data cubes.

4. Instrumental Limitations

In this section we review instabilities, nonreproducibilities, and nonideal behaviors of some components of the system and estimate their effects on the radiometric accuracy. Most of these effects either have been solved technically or can be calibrated with specific procedures to be described in detail in Part 2.[17]

A. Radiometric Fluctuations

1. *Source and Detectors*

The light output of the quartz tungsten halogen lamp is perfectly stable over days (±0.05% peak-to-peak) thanks to the light-intensity controller. However, over longer periods the signal output of the visible detector slightly drifts with an amplitude of approximately 0.15%. Changes of the ambient temperature cause this variation. The measured global temperature-dependent drift of the visible detector and its associated electronic devices is approximately −0.025%/°C, much smaller than expected from the specifications of the optoelectronic components. Consequently, for a stabilized room temperature of ±1 °C, the signal variations will be less than 0.1%. The Si reference detector has a similar sensitivity to temperature. The InSb infrared detector, actively cooled at 80 K, also displays a similar long-term drift of its signal, essentially because of its electronics.

2. *Fiber Optics*

Optical fibers are used to carry the light from the monochromator to the goniometer (see Section 3). The choice of fluoride glass fibers was based on their excellent transmission from the visible to the IR. To better characterize the fiber bundle, we measured its transmission with the monochromator to ensure that there is no strong absorption in the UV. Its attenuation was found to be lower than 1 dB m^{-1} over most of the spectral range (350–4500 nm). When convolved with the source output spectrum and the electro-optical efficiencies of all the illumination and detection components, the system delivers a measurable signal between 310 and 4800 nm. However, a S/N ratio larger than 100 is obtained in 1 s (time constant of the lock-in amplifier) and for the larger slit width (1500 μm) only in the 380–3900-nm range (Fig. 4). For a better S/N ratio, especially outside that range, a larger time constant or coaddition of successive measurements is requisite. When the goniometer is in the cold room (−35 °C), it is anticipated that the S/N ratio above 3000 nm will be significantly improved owing to reduced background thermal radiation.

The curvature of the fibers varies as a function of the incidence angle (θ_i) of the illumination beam, inducing small light-intensity variations. To evaluate the angular-dependent illumination and to correct this effect, we positioned the calibrated reference

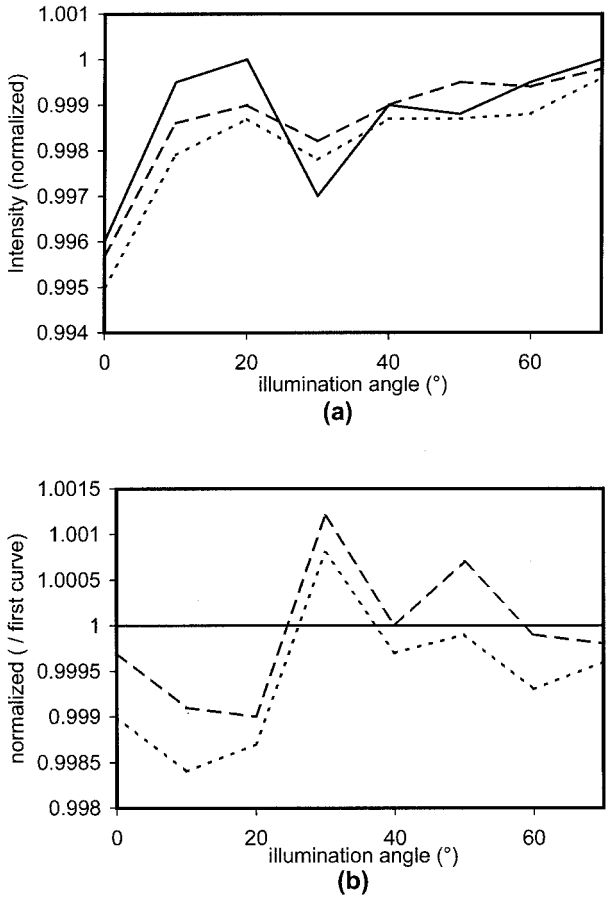

Fig. 5. Light-intensity variations induced by fiber-optic curvature. (a) Illumination intensity as a function of the incident angle θ_i. Three independent measurements are shown. (b) Ratio of the second and third measurements relative to the first one. An angular dependency of 0.5% and a nonreproducibility of less than $\pm 0.2\%$ are observed.

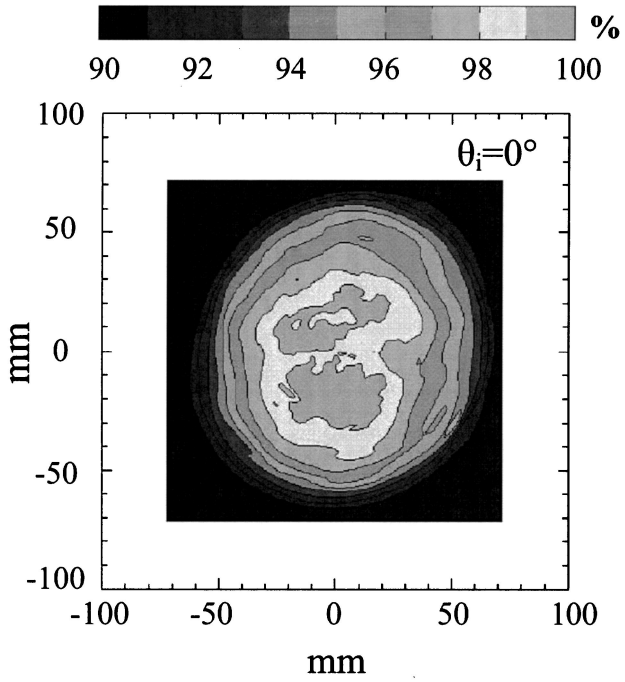

Fig. 6. Spatial homogeneity of the illumination beam at the sample surface for vertical illumination (λ = 700 nm). The contour curves express the irradiance in percents relative to the maximum value.

detector in the center of the illumination beam. Three series of measurements acquired when the illumination arm moved from 0° to 70° are shown in Fig. 5(a). In addition to the angular-dependent variation of the illumination (0.5%) due to the fiber-optic curvature, a nonreproducible variability ($<\pm 0.2\%$) at fixed incidence is observed [Fig. 5(b)]. A calibration procedure to fully correct for these radiometric effects will be described in Part 2.[17]

B. Homogeneity of the Illumination

The spatial homogeneity of the divergent light beam that emerges from the monochromator is, for the most part, determined by the input illumination conditions. Similarly, the spatial characteristics of the parallel illumination beam are strongly influenced by both the fiber-optic input illumination and the fibers' curvature. In general, light intensity slowly decreases from the center of the beam. To estimate the homogeneity of the illumination beam, we scanned the illuminated surface with a small silicon detector (1 mm $\times$ 1 mm) mounted on *XY* motorized linear stages. Measurements were performed at zenith incidence (Fig. 6). This position can be considered as the worst situation because homogeneity improves as the illumination angle increases, owing to the expansion of the illumination pattern along the principal plane. Spatial variation of the light intensity inside the area viewed by the detectors was found to be typically less than 2% at nadir (20 mm in diameter, $\theta_r = 0°$) and to as much as 70° observation at all azimuths (diameter: 60 mm). At some wavelengths the inhomogeneities reach 3% in the nadir observation and to as much as 4% for $\theta_r = 70°$. Within these limits ($\theta_r \leq 70°$), the homogeneity fluctuations over all θ_r and all wavelengths approached 4%, but the variation of its integrated intensity in the observation spot did not exceed 0.3%. When the incidence angle is changed, the typical local fluctuations of the map were 1%, but the maximum integrated intensity changes in the observation spot and over the reference detector area was 0.5% (see Subsection 4.A.2). A calibration protocol has been developed to take into account the beam homogeneity map for all combinations of illumination and observation angles. It will be presented in Part 2.[17]

C. Polarization of the Illumination

For an unpolarized input, the light output from the monochromator is partially polarized owing to the grating characteristics. The efficiency of a grating for the *P* (radiation with the electric field vector parallel to the grating grooves) and *S* components (perpendicular) strongly varies over the spectral range (Fig. 7). When the light travels inside the fiber op-

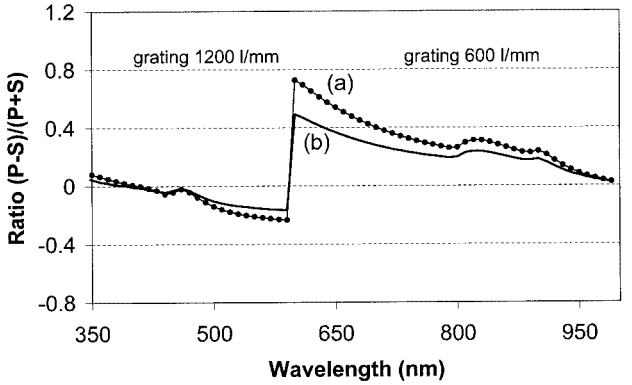

Fig. 7. Polarization: ratio $(P - S)/(P + S)$ of the P (radiation with the electric field vector parallel to the grating grooves) and S (perpendicular) components of the light (a) at the exit of the monochromator and (b) at the center of the illumination beam. l/mm, lines/mm.

tics, it is partly depolarized. To estimate this effect, we measured the two components of the partially polarized light at the output of the monochromator and in the center of the illumination beam (Fig. 7). We also measured the homogeneity of the beam for both polarized components at several wavelengths (Fig. 8). The measurements indicate that the light output from the fibers is still partly polarized (mainly in the center of the beam, in which only 25%–30% of the flux is depolarized by the fibers) and that the depolarization efficiency depends on the curvature of the fibers (the polarization decreases for smaller curvature radius). The homogeneity of the radiance in the beam also progressively decreases with the curvature radius of the fibers. Considering that the depolarization of the illumination beam comes at the price of its homogeneity, we decided to favor homogeneity and to address the polarization issue by adding the Glan–Thompson polarizer at the output of the fibers (see Subsection 3.B). A relatively homogeneous and perfectly polarized beam at all wavelengths (between 320 and 3000 nm) is thus obtained. At wavelengths in which the output flux from the monochromator is only slightly polarized (e.g., for $(P - S)/(P + S) \leq 0.25$, see Fig. 7), the inhomogeneity maps of the P_i (radiation with the electric field vector parallel to the sample surface) and S_i (perpendicular to P_i) components are similar: spot integrated difference $\leq 0.2\%$ [Fig. 8(b)]. However, when the polarization is larger (e.g., between 600 and 700 nm, see Fig. 7), the local differences between P_i and S_i can reach several percents, with observation spot differences exceeding 1% [Fig. 8(a)]. Thus the calibration procedure must consider the inhomogeneity maps of both polarizations (see Part 2[17]). The combination of reflectance measurements for the two orthogonal polarizations of the illumination should enable us to reconstruct the unpolarized situation. This configuration also gives us the capability to study the reflectance behavior of each polarization component independently.

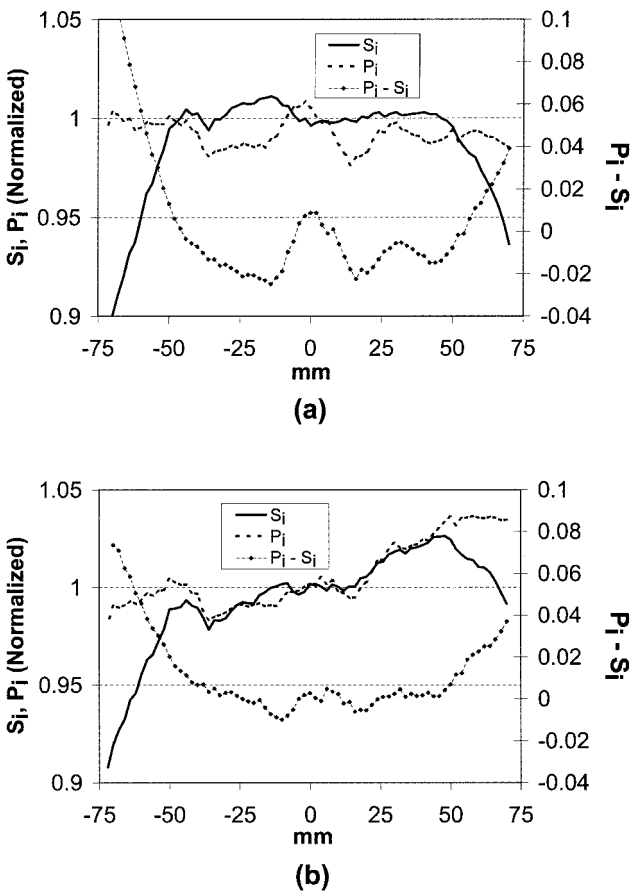

Fig. 8. Homogeneity of the illumination beam (in the principal plane) for both P_i (radiation with the electric field vector parallel to the sample surface) and S_i (perpendicular to P_i): (a) at 700 nm and (b) at 900 nm. Both S_i and P_i are normalized to 1 in the center of the beam.

D. Mechanical Adjustments

A major difficulty was accurately positioning the optical components fixed to the goniometer arms (fiber-optic bundle, paraboloidal reflector, and detector assemblies). Three micrometer linear stages assembled in an *XYZ* configuration were used to precisely position the fiber output at the focal point of the off-axis paraboloidal reflector, itself first adjusted to make the central axis of the illumination beam intersect the center of the sample surface, at all incidence angles.

Alignment of the detector optical axes is much more critical. Even a small misadjustment produces a notable drift of the center of the sample area viewed by the detectors when the observation arm moves toward high observation angles, especially above 60°. To perform the alignment, we placed a grid on the sample surface plane to measure the axis drift of each detector. The observation arm was positioned at −70°, and the center of each detector field of view was determined. A second measurement was performed at +70°. The positions of the silicon (UV–visible) and InSb (IR) detectors were optimized to obtain a maximum axis drift of 2 mm between

−70° and +70° as well as a maximum shift of 1 mm between the centers of the visible and IR detector fields of view. These adjustments are especially important for good stability and knowledge of the position of the observation spots relative to the inhomogeneity map of the illumination, at all angles, for an accurate correction of this inhomogeneity (see Part 2[17]).

5. Conclusion

We have presented the design and tests of a new, to our knowledge, spectrogonio radiometer to measure the bidirectional reflectance and polarization functions of planetary surface materials (down to −35 °C). It can provide spectral BRDF measurements from the visible to the near IR (310 to 4800 nm) of granular and compact surfaces made of various types of material. The illumination beam can be fully polarized with variable orientations.

The instrument has no strong constraint on the illumination angle in the 0°–90° range, except that the illumination of the surface varies as cos θ_i and thus, to the first order, the S/N ratio of the reflected radiance. In contrast, the observation geometry has no direct effect on the S/N ratio but is radiometrically limited to emergence angles below 80° (azimuth: 0°–180°) for large-grained translucent materials. If necessary, this range can be extended to 83° but with a smaller solid angle (<1°) for observations of dark or fine-grained materials. The main geometric limitation is the phase angle between the illumination and the observation (minimum of 8° for coarse-grained transparent materials, 4.5° for fine-grained or dark materials). The detailed characteristics of the instrument are summarized in Table 1. The major novel feature of this instrument is that it is capable of measuring dark to translucent materials with a high degree of radiometric accuracy over wide angular ranges.

However, this was achieved only through the development of several spectral and radiometric calibration protocols,[18] described in Part 2,[17] that were required to overcome the various limitations and instabilities of the system reported in this paper. Our aim is to obtain bidirectional reflectance data with an absolute radiometric accuracy better than 1% over the whole spectral and angular ranges. This precision has been already achieved in the spectral range from 400 to 1000 nm (see Part 2).[17,18]

This spectrogonio radiometer should provide accurate laboratory data sets to validate and improve the theories of light scattering and polarization by planetary surfaces. In particular, we hope to determine the range of validity of our radiative transfer model for the analysis of planetary surface hyperspectral images.[3]

It will also provide detailed bidirectional reflectance measurements of several types of material such as ices and minerals to supply a spectral BRDF database. An extensive study of the dependence of the spectral BRDF of sulfur surfaces with material texture has been already performed in the visible range.[18] It shows the high quality of the data and the strong scientific potential of the instrument for BRDF studies.

We thank Pierre Kern of the Laboratoire d'Astrophysique de l'Observatoire de Grenoble and Claude Sergent of the Centre d'Etude de la Neige for suggestions and discussions throughout the design of the instrument. Will Grundy thanks the French Ministère des Affaires Etrangères for a Châteaubriand postdoctoral fellowship. The spectrogonio radiometer was funded by the French Programme National de Planétologie and Programme National de Télédédection Spatiale, the Program Emergence of the Région Rhône-Alpes, the University Joseph Fourier of Grenoble (Bonus Qualité Recherche), the Institut National des Sciences de l'Univers of the Centre National de la Recherche Scientifique and, not the least, the Centre National d'Etudes Spatiales.

References

1. B. Hapke, *Theory of Reflectance and Emittance Spectroscopy* (Cambridge U. Press, New York, 1993).
2. K. Stamnes, S. Tsay, W. Wiscombe, and K. Jayaweera, "Numerically stable algorithm for discrete-ordinate-method radiative transfer in multiple scattering and emitting layered media," Appl. Opt. **27,** 2502–2509 (1988).
3. S. Douté and B. Schmitt, "A multilayer bidirectional reflectance model for the analysis of planetary surface hyperspectral images at visible and near-infrared wavelengths," J. Geophys. Res. E **103,** 31367–31389 (1998).
4. W. M. Grundy, S. Douté, and B. Schmitt, "A Monte Carlo ray-tracing model for scattering and polarization by large particles with complex shapes," J. Geophys. Res. E **105,** 29291–29314 (2000).
5. B. J. Buratti, W. D. Smythe, R. M. Nelson, and V. Gharakhani, "Spectrogoniometer for measuring planetary surface materials at small phase angles," Appl. Opt. **27,** 161–165 (1988).
6. R. M. Nelson, B. W. Hapke, W. D. Smythe, and L. J. Horn, "Phase curves of selected particulate materials: the contribution of coherent backscattering to the opposition surge," Icarus **131,** 223–230 (1998).
7. R. M. Nelson, B. W. Hapke, W. D. Smythe, and L. J. Spilker, "The opposition effect in simulated planetary regoliths. Reflectance and circular polarization ratio change at small phase angle," Icarus **147,** 545–558 (2000).
8. S. Kaasalainen, J. Piironen, K. Muinonen, H. Karttunen, and J. Peltoniemi, "Laboratory experiments on backscattering from regolith samples," Appl. Opt. **41,** 4416–4420 (2002).
9. C. M. Pieters, "Strength of mineral absorption features in the transmitted component of near-infrared light: first results from RELAB," J. Geophys. Res. B **88,** 9534–9544 (1983).
10. C. Koechler, B. Hosgood, G. Andreoli, G. Schmuck, J. Verdebout, A. Pegoraro, J. Hill, W. Mehl, D. Roberts, and M. Smith, "The European Optical Goniometric Facility: technical description and first experiments on spectral unmixing," in *Proceedings of International Geoscience and Remote Sensing Symposium*, E. Njoku and J. Way, eds. (Institute of Electrical and Electronics Engineers, New York, 1994) pp. 2375–2377.
11. S. Sandmeier, C. Müller, B. Hosgood, and G. Andreoli, "Sensitivity analysis and quality assessment of laboratory BRDF data," Remote Sens. Environ. **64,** 176–191 (1998).
12. S. Sandmeier and K. I. Itten, "A field goniometer system (FIGOS) for acquisition of hyperspectral BRDF data," IEEE Trans. Geosci. Remote Sens. **37,** 978–986 (1999).
13. T. H. Painter, "The hyperspectral bidirectional reflectance of

snow: modeling, measurement, and instrumentation," Ph.D. thesis (University of California, Santa Barbara, California, 2002).
14. G. Serrot, M. Bodilis, X. Briottet, and H. Cosnefroy, "Presentation of a new BRDF measurement device," in *Atmospheric Propagation, Adaptive Systems, and Lidar Techniques for Remote Sensing II*, A. D. Devir, A. Kohle, U. Schreiber, and C. Werner, eds., Proc. SPIE **3494,** 34–40 (1998).
15. Y. Boucher, H. Cosnefroy, D. Petit, G. Serrot, and X. Briottet, "Comparison of measured and modeled BRDF of natural targets," in *Targets and Background: Characterization and Representation V*, W. R. Watkins, D. Clement, and W. R. Reynolds, eds., Proc. SPIE **3699,** 16–26 (1999).
16. A. Oehler, "Experimentelle und theoretische Untersuchung der goniospektrometrischen Eigenschaften regolithartiger Materialen in den Spektralbereichen UV, VIS, und NIR," Ph.D. thesis (Institut für Planetenerkundung, Deutsche Forschungsanstalt für Luft- und Raumfahrt, Berlin, 1996).
17. N. Bonnefoy, Laboratoire de Planétologie de Grenoble, Bâtiment D de Physique, B.P. 53, 38041 Grenoble Cedex 9, France, and B. Schmitt, O. Brissaud, and S. Douté, are preparing a manuscript, "Spectrogonio radiometer for the study of the bidirectional reflectance and polarization functions of planetary surfaces. 2. Spectral and radiometric calibrations."
18. N. Bonnefoy, "Développement d'un spectro-goniomètre pour l'étude de la réflectance bidirectionnelle des surfaces géophysiques. Application au soufre et perspectives pour le satellite Io," Ph.D. thesis (Laboratoire de Planétologie de Grenoble—Université Joseph Fourier, Grenoble, 2001).